Coupled data-driven and process-based model for fluorescent dissolved organic matter prediction in a shallow subtropical reservoir

Xinchen Wang [1, 2], Hong Zhang [1, 2,*], Edoardo Bertone [1, 2], Rodney A. Stewart [1, 2] and Sara P. Hughes[3]

[1] School of Engineering and Built Environment, Griffith University, Queensland 4222, Australia; xinchen.wang@griffith.edu.au (X.W.); hong.zhang@griffith.edu.au (H.Z.); e.bertone@griffith.edu.au (E.B.), r.stewart@griffith.edu.au (R.S)

[2] Cities Research Institute, Griffith University, Queensland 4222, Australia

[3] Catchment Science, Seqwater, 117 Brisbane St., Ipswich, Queensland 4305, Australia; Sara.PetersHughes@seqwater.com.au (S. H.)

***** Correspondence: hong.zhang@griffith.edu.au (H.Z.); Tel.: +61-7-5552-9015

Abstract

Monitoring and understanding the dissolved organic matter (DOM) cycle in a drinking water reservoir is crucial to water authorities, since most water treatment practices aim to remove DOM to prevent the formation of potentially harmful disinfection by-products. A vertical profiling system (VPS) installed in reservoirs can continuously detect the fluorescent DOM (fDOM) and determine the fDOM transport process. Although the VPS can interprete fDOM concentrations, water treatment operators still collect and rely upon DOM datasets that are manually sampled throughout the year. A long-term historical database provides an opportunity to develop a three-dimensional fDOM prediction model. In the present study, we collected and analysed VPS and sampling data and developed and assessed an innovative coupled data-driven and process-based model. These models were able to forecast future fDOM in both temperate and extreme weather conditions. Modelling scenario analysis concluded that deeper layers of the reservoir as well as areas close to the riverine zone had higher fDOM concentrations than any other zones during storm events. Simulated fDOM can be a proxy for dissolved organic carbon concentration. The model also determined that inflow creeks were predominant fDOM sources during storm events and continuing winds transported the fDOM from bottom to surface water layers. This study has implications for reservoir and water treatment plant operators seeking to gain a better understanding of the DOM cycle in a reservoir and to more efficiently manage DOM removal.

Keywords: Dissolved organic matter; vertical profiling system; transport processes; mixing processes.

Software and data availability:

Name of software: MIKE3 Flow Model; MATLAB

Developer: Danish Hydraulic Institute (DHI); MathWorks

Contact information: Agern Allé 5, Hørsholm 2970 Denmark; +45 45169333 Telephone; +45 45169292 Fax; mike@dhigroup.com;

Apple Hill Dr, Natick, MA 01760 USA; 508-647-7000 Telephone; +1-508-647-7001 Fax

Year first available: 2016 (Window 10, 64bit version)

Hardware required: Microsoft Window 7 professional Service Pack 1 (64bit) and Windows 10 Pro (64bit)

Software required:

Processor	3 GHz PC (or higher)
Memory(RAM)	2GB (or higher)
Hard disk	40GB (or higher)
Graphics card	64 MB RAM (256MB RAM or higher)

Availability and cost: MIKE3 Flow Model license is provided by DHI, Australia; MATLAB license is provided by MathWorks.

Software program language: Main program (FORTRAN), front-end (C). Source code not provided.

1. Introduction

Dissolved organic matter (DOM) is an important component of source water worldwide. With variables in biogeochemical environments and water resources (e.g., temperature, pH, biological process and organic matter source), the composition of aquatic DOM varies considerably in molecular size, molecular weight (from hundreds to millions of daltons), solubility, lability and structure (Fabris, Chow, Drikas, & Eikebrokk, 2008; Gjessing, 1976; Leenheer & Croué, 2003). DOM comprises soluble organic materials, such as organic forms of carbon, nitrogen, sulfur and phosphorus, released by the degradation of plants, animals and microorganisms (Zhang et al., 2012). In lakes and reservoirs, three major sources of DOM are autochthonous (aquatic), allochthonous (terrestrial) and synthetic (industrial or manmade), with seasonally variable compositions (Mostofa, 2013). Researchers have found that DOM imparts colour, taste and odour (Lambert & Graham, 1995; Worrall & Burt, 2010), pollutes and blocks the membranes and filters of water treatment plants (Huber, 1998), decreases the light penetration of water and influences biological growth in aquatic systems (Ask et al., 2009; Moran & Zepp, 1997). Furthermore, in the process of treating drinking water, if hydrophilic DOM in raw water bypasses the treatment processes, by reacting with chlorine in the distribution system it can result in the formation of potentially dangerous disinfection by-products, the most common being the trihalomethanes (Pagano, Bida, & Kenny, 2014), which are also considered carcinogenic (Palmstrom, Carlson, & Cooke, 1988). Hence, a high DOM concentration in a water system used for drinking water is a significant concern.

A more thorough understanding of the DOM distribution and the variables affecting it would allow water authorities to more efficiently manage DOM treatment. Fluorescence spectroscopy is a proven technique to characterise the composition of aquatic DOM composition. Lee et al. (2015), Mast, Murphy, Clow, Penn, and Sexstone (2016) and Khamis et al. (2017) found that the relationship between dissolved organic matter (DOC) and peak C (in the blue and green fluorescence regions, the excitation is 300-350 nm and the emission is 400-500 nm) is strong. Cyr et al. (2017) suggested that primary production is complex in water related system and proved that fDOM is a good proxy for processes influencing the DOM pool. Researchers agree that fluorescence measurements are proxies for chemical and biological DOM (Carstea, Popa, Baker, & Bridgeman, 2019). Probes measuring the fluorescent signal of DOM have recently been developed and installed in several Australian reservoirs, providing high-frequency estimations of fluorescent DOM (fDOM) in lakes. These probes take in-situ optical measurements using long-term and field-deployable fluorometers, which enable researchers to collect high-resolution temporal data (Ruhala & Zarnetske, 2017). In-situ submersible fDOM fluorometers have been widely used in published field studies to date (De Oliveira et al., 2018; Pellerin et al., 2012; Saraceno et al., 2009; Wang,

Zhang, Bertone, Stewart, & O'Halloran, 2019). While wavelength scanning fluorometers measure emission signals over a range of wavelengths and are more reliable, fDOM fluorometers use a light-emitting diode as a light source and have a single fixed excitation-emission wavelength pair (Lee et al., 2015; Saraceno et al., 2009). Fluorescence sensors allow high-resolution measurements of fDOM in rivers and reservoirs during storm events (Carstea et al., 2019). However, when monitoring fDOM concentrations using a fluorometer, the optical signal of the fDOM probe is interfered and distorted by temperature, turbidity, pH, salinity and inner filter effects. Turbidity is an inherent issue for fDOM sensors as it fundamentally interferes with light passage and detection (Ruhala & Zarnetske, 2017). The type of turbidity is also important, where the magnitude of fDOM signals bias is related to the shape and size of suspended particles (De Oliveira et al., 2018; Saraceno, Shanley, Downing, & Pellerin, 2017). An increase of turbidity leads to an increased amount of scattering of the excitation light emitted by the fDOM sensor, which causes the decline of the light available in the sampling volume to excite fDOM (Downing, Pellerin, Bergamaschi, Saraceno, & Kraus, 2012). Apart from turbidity, the present of fDOM in the particulate organic matter (POM) fraction, especially the protein-like fDOM, also distort the fDOM signal. Researchers found that the florescence of POM increases the fDOM (Korak, Wert, & Rosario-Ortiz, 2015; Stedmon et al., 2007). On the other hand, the higher temperatures increase the probability of an excited electron to return to its ground state by radiationless decay, which decreases fluorescence intensity (Henderson et al., 2009). Hence, it is necessary to quantify turbidity and temperature interferences to achieve more reliable fDOM readings. Though still affecting the readings, previous work showed that pH and salinity have a more minor effect in a fDOM sensor accuracy, and inner filtering effect becomes relevant when the absorption coefficient of CDOM is high (> 10 m^{-1}) (De Oliveira et al., 2018).

In lakes and reservoirs, a fDOM probe can be installed in vertical profiling system (VPS), and moves up and down the water column, collecting one-dimensional vertical measurements of fDOM, at every 1-3m depth, usually once a hour depending on reservoir depth. Although probes measuring fDOM have been widely used in lakes, they are unable to describe the DOM distribution in three dimensions.

In terms of drinking water management, modelling can be used prior to field observation to provide information on the contribution of different sources of DOM concentration in the raw water intake of a water treatment plant. Water operators are required to establish efficient, reliable and safe models to predict and reduce high DOM concentrations in water before it can be distributed as a potable supply to consumers. Numerical models are suitable methods for water quality prediction, and many numerical models for aquatic systems have been used to simulate organic matter concentrations. Sato et al. (2007) established numerical marine ecosystem models and simulated the organic matter concentrations in

Lake Saroma, Japan. In their study, particulate and dissolved organic matter were simulated, and each type was modelled as two degradable fractions (labile and refractory) with various mineralisation rates to illustrate the decrease in reactivity over time (Sato et al., 2007). This ecosystem model considered the loading of organic matter from rivers and the exudation of phytoplankton (Sato et al., 2007). Sato et al. (2007) found that storm events supplied organic matter and nutrients into the lake, and typhoons influenced the organic matter settling to the bottom of the lake. Furthermore, Druon et al. (2010) modelled the dynamics and export of DOM on the U.S. continental shelf. The DOC concentrations in this study were based on phytoplankton exudation, solubilisation of small and large carbon detritus and remineralisation of the semi-labile DOC (Druon et al., 2010). These researchers concluded that the DOM was closely linked to the residence time of water masses of its distribution and export water masses (Druon et al., 2010). Another model was developed by Liungman and Moreno-Arancibia (2010) for the Himmerfjärden Estuary, Sweden. The study indicated that sediment processes can impact the phytoplankton and detritus that settle and reach the bottom of a body of water, and this influences the inorganic matter which is released from sediments. Previous DOM models are complex and most of them only consider the biochemical process of DOM, such as phytoplankton exudation and remineralisation of labile DOM. They are calibrated and verified based on low-frequency water sampling data. Previous DOM models are limited to the simulation of horizontal DOM variation and do not fully consider the hydrodynamic and sediment transport process effects on DOM transport processes.

To date, according to the Authors' knowledge, there has been no attempt to build a three-dimensional (3D) coupled data-driven and process-based model through high-frequency and in-situ optical DOM measurements in the lake systems. Therefore, for this study, after extensive data collection from several sources and over several years, we established a coupled data-driven and process-based model for fDOM prediction for the Tingalpa Reservoir, Australia. The developed fDOM prediction model considers the effects of hydrodynamic and sediment transport processes. Model performance and accuracy could be calibrated and verified using available high-frequency monitoring data from the VPS. Moreover, the fDOM prediction model can be used to analyse the fDOM distribution in both horizontal and vertical directions and predict the timing and peak DOM concentration, especially during extreme events. This innovative model is a general method of understanding and predicting 3D fDOM distributions in any reservoir or lake with high frequency fDOM monitoring instrumentation in place.

2. Study site and monitoring data

To demonstrate the feasibility of the developed comprehensive model, a shallow, subtropical reservoir, i.e. the Tingalpa Reservoir was selected as the study site. The Tingalpa Reservoir is located in South East Queensland (SEQ), Australia (153.18°E, 27.53°S). It provides approximately 20% of the water to Redland City. The Leslie Harrison Dam is located on the north eastern side of the reservoir. The surface area covers approximately 470 hectares, and the catchment area is 87.5 km^2. There are two main inflows: the Tingalpa Creek from the south east, and the Stockyard Creek from the south west. Seqwater, the bulk water supply authority for SEQ, manages the reservoir treatment operations. To achieve higher risk mitigation for dam safety, Seqwater reduced the reservoir water storage to 13,206 ML on 1 August 2014. Previous studies have shown that when rewetting occurs after a long dry period, the organic matter contents in the reservoir increased and affected the water quality; higher organic matter concentrations resulted from decaying macrophytes in the sediment soils that are transported to the water (Lu, Faggotter, Bunn, & Burford, 2017).

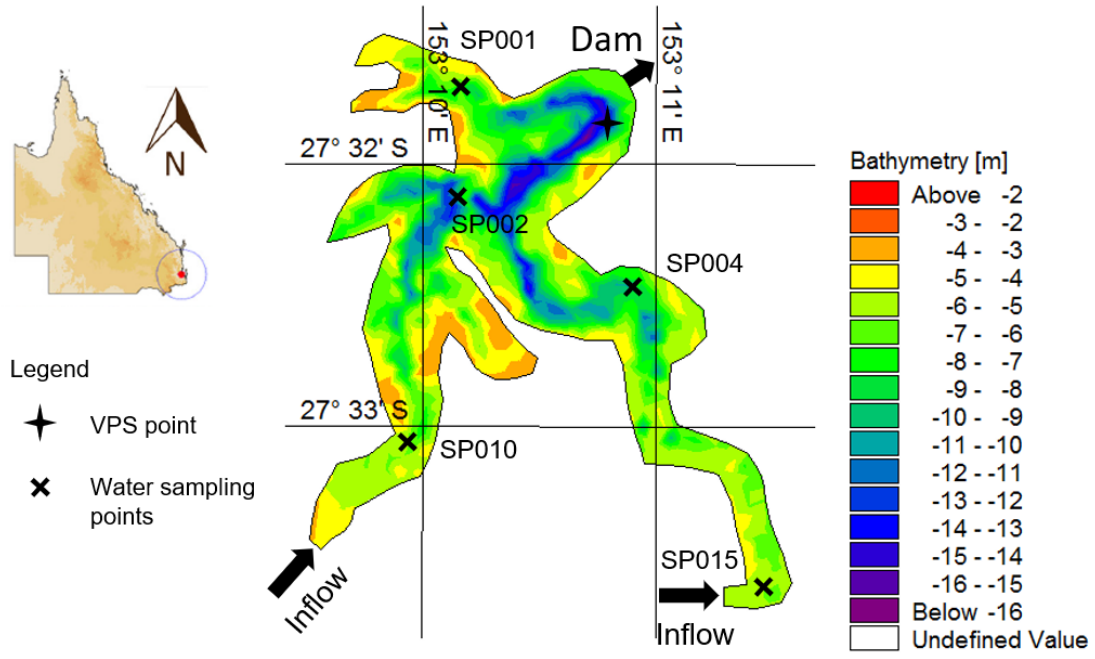

Figure 1. Monitoring sites in the Tingalpa Reservoir and the reservoir's bathymetry [m AHD].

Water quality in the Tingalpa Reservoir is monitored mainly through laboratory analysis of monthly manually collected water samples. In 2013, a VPS was installed 500 m from the Leslie Harrison Dam, as shown in Figure 1. A set of water quality probes in the VPS automatically winches up and down in the water column and measures water quality variables, including water temperature, pH, dissolved oxygen (DO), conductivity, turbidity and fDOM. The fDOM was measured using an EXO fDOM Smart Sensor (YSI, Yellow Springs, OH, USA) which has 365±5nm excitation and 480±40nm emission wavelength to

estimate the quantity of fluorescent, humic-like DOM (peak C), and it is reported as relative fluorescence units (RFU) or quinine sulphate units (QSU) (Xylem, 2019).

Seqwater has provided physical and chemical data for the Tingalpa Reservoir, collected both through water samplings and by the VPS. Manual water samplings at the raw water inlet are taken weekly, while the water samplings at monitoring stations are taken monthly on the lake. The water sampling points are shown in Figure 1. Moreover, previous studies conducted by our reseach group (De Oliveira et al., 2018) conducted water sampling to measure the fDOM and DOC concentration from May 2017 to September 2017 in the Tingalpa Reservoir. Data from the VPS have been available since the VPS was installed (i.e. 2013), and several types of manual sampling data have been available since 2010. Other parameters were collected from the Australian Bureau of Meteorology and the Commonwealth Scientific and Industrial Research Organization (CSIRO). This organization provided the inflow parameters for Tingalpa Creek. Table 1 provides a list of the available data.

Table 1. Sources and features of the available data.

Variable	Source	Method	Frequency	Period
DOC	Seqwater	Water sampling in raw water inlet	Weekly	2010-2019
SUVA			Weekly	2013-2019
UV_{254}			Weekly	2010-2019
TOC			Weekly	2010-2019
Suspended Solids			Monthly	2017-2019
Temperature			Weekly	2011-2019
Turbidity			Monthly	2010-2019
pH			Weekly	2010-2019
Conductivity			Weekly	2010-2019
DOC	Seqwater	Water sampling at monitoring station	Monthly	2010-2019
TOC			Monthly	2010-2019
Suspended Solid			Monthly	2010-2019
Total Dissolved Phosphorus			Monthly	2010-2019
Total Dissolved Nitrogen			Monthly	2010-2019
DO	Seqwater and VPS[a]	Water sampling at monitoring station, VPS	Monthly, Hourly	2010-2019, 2013-2019
Temperature			Monthly, Hourly	2010-2019, 2013-2019
Turbidity			Monthly, Hourly	2010-2019, 2013-2019
pH			Monthly, Hourly	2010-2019, 2013-2019

Conductivity			Monthly, Hourly	2010-2019, 2013-2019
fDOM	VPS	VPS	Hourly	2013-2018
Air Temperature	BoM[b]	Data with fee	Hourly	2013-2019
Wind Speed and Direction			Hourly	2013-2019
Rainfall			Hourly	2013-2019
Solar Radiation			Hourly	2013-2019
Relative Humidity			Hourly	2013-2019
Outflow	Seqwater		Daily	2013-2017
Inflow	Seqwater		Hourly	2015-2017
Inflow Temperature			Hourly	2015-2017
Inflow Turbidity			Hourly	2015-2017
Inflow pH			Hourly	2015-2017
Inflow DO			Hourly	2015-2017

[a] Vertical Profiling System, Tingalpa Reservoir.
[b] Australian Bureau of Meteorology.
[c] Commonwealth Scientific and Industrial Research Organization.

3. Dissolved organic matter cycle in freshwater reservoirs

Reservoirs are complex biogeochemical systems in which production, transformation and loss of organic matter occur simultaneously (Kraus et al., 2011). The net effects of these processes are determined by certain factors, including algal and bacterial activity, inflow DOM quantity and composition, nutrient availability, storm events, temperature, solar radiation and pH (Holland, Stauber, Wood, Trenfield, & Jolley, 2018; Kraus et al., 2011; Mash, Westerhoff, Baker, Nieman, & Nguyen, 2004; Zepp, Erickson Iii, Paul, & Sulzberger, 2007). Chromophoric DOM is the optically measurable component of DOM, and fDOM refers to the chromophoric DOM that fluoresces. The common fluorescence type are peak T (in the ultraviolet absorbance fluorescence region, the excitation wavelength is ~230 and ~275 nm and the emission wavelength is ~340 nm) and peak C (Coble, 1996; Hudson, Baker, & Reynolds, 2007). Peak T refers to the tryptophan-like DOM, and peak C refers to the humic-like DOM. In the literature, peak C is a proxy for the broader DOC and relates to the substances with highly aromatic and mainly high molecular weight components (Jiang et al., 2017; Ruhala & Zarnetske, 2017).

The key processes involved in a lake's DOM cycle are summarised in Figure 2. There are evident differences in the DOM distribution between the surface and bottom layers of a water column. In the surface water, radiation promotes photosynthesis and causes a high level of DO (Tundisi & Tundisi, 2012). The presence of algae means a high pH because the

algae removes acidic CO_2 forms such as HCO_3^- (Dubinsky & Rotem, 1974). Algal production in surface waters contributes to the amount of DOM present, especially DOM with a low molecular weight (Kraus et al., 2011). In the colder bottom water, light cannot penetrate, nor can algae develop or produce oxygen through photosynthesis, and the water is typically acidic and contains little or no DO for bacteria respiration (Tundisi & Tundisi, 2012). Holland et al. (2018) found acidic waters are dominated by DOM that is aromatic and humic-like with a high molecular weight. Under stratified conditions, the DOM quantity and composition vary in vertical distribution between the surface and bottom waters. The stratification of DOM depends on the depth of the reservoir/lake. If the lake is shallow, the stratification of DOM quantity and composition in the vertical direction is not obvious.

The water dynamics of the lake also alters the DOM cycle. Lower water residence times where respiration exceeds photosynthesis, provide an opportunity for the environmental consumption process of DOM (Jack, Sellers, & Bukaveckas, 2002; Kraus et al., 2011). Higher water residence times enable the mixing of fluent waters and the stabilisation of the DOM's quality (Awad et al., 2016). Inflow's influence on the DOM cycle occurs mainly during storm events. Rainfall increases the river inflow and the terrestrial DOM inputs into the reservoir, leading to high fDOM concentration, and the degree of increase varies according to the frequency and quantity of precipitation (Bergamaschi et al., 2012; Bertuzzo, Helton, Hall Jr, & Battin, 2017; Carstea, 2012; Mihalevich, Horsburgh, & Melcher, 2017; Tunaley, Tetzlaff, Lessels, & Soulsby, 2016). There is a delayed input of high DOM concentrations from the surface of the water, from shallow flow paths on the hillslope and from riparian sources.

Many studies have found that fDOM concentration lags behind turbidity and discharge and varies from site to site in the river catchment, with a lag ranging from 1 hour (h) to 1 day. Pellerin et al. (2012) reported that peak fDOM concentration lagged behind peak streamflow by less than 1 h for a 2-day 35 mm rainfall event. Saraceno et al. (2009) study showed that during a 4-day 44 mm rainfall event, peak fDOM lagged behind peak discharge by 9 h. In addition, Bergamaschi et al. (2012) found that fDOM concentration lagged a full day behind peak discharge in 2-day 80 mm rainfall. These studies found that the lag between peak discharge and peak fDOM concentration is correlated with the rainfall amount. The lag of the fDOM peak relative to the turbidity peak suggests that the relative importance of shallow soil drainage remains elevated for several days after an event (Saraceno et al., 2009).

The DOM present in the reservoir waters during the wet season has a high percentage of humic-like and aromatic organic compounds, which makes fDOM readings an accurate representation of DOM, since it has been proved that fDOM is related to aromatic and humic-like DOM components. (Awad et al., 2016; Carstea, 2012; Stutter, Dunn, & Lumsdon, 2012). Previous studies have also found that measurements of in-situ fDOM are good proxies for

the DOM concentration during storm events (Saraceno et al., 2009). As a consequence, the focus of this study was on understanding the DOM dynamics during wet weather events, as the available fDOM data can be considered a good proxy of the overall DOM concentrations during such critical events for the DOM cycle.

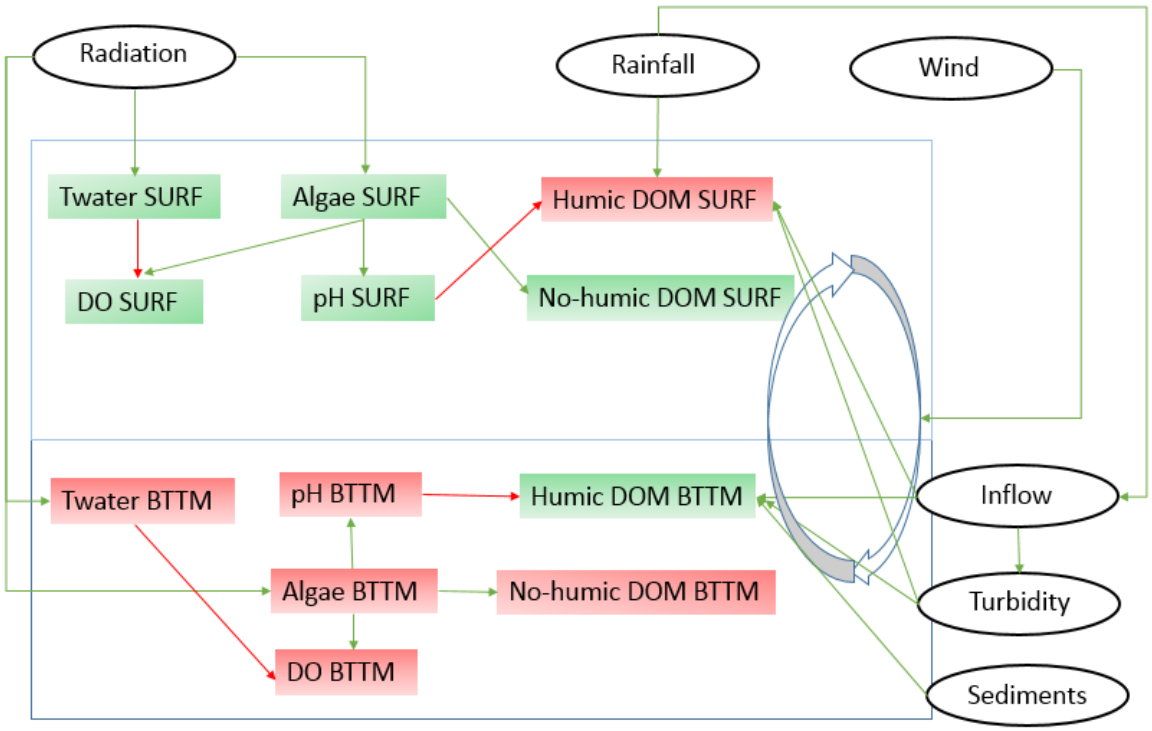

Figure 2. Schematisation of the DOM cycle in a reservoir. Green connections: an increase in x increases in y; red connections: an increase in x decreases in y; upper box: surface (SURF) water; lower box: bottom (BTTM) water; rectangles: variables part of the cycle (green rectangles: high concentrations under stratification; red rectangles: low concentrations under stratification); ovals: external inputs; curved arrow: the vertical water mixing; Twater: water temperature.

4. Method

4.1 Coupled data-driven and process-based model

Three-dimensional hydrodynamic, sediment-transport and data-driven models were developed to achieve the 3D fDOM prediction. The inputs to the 3D hydrodynamic and sediment transport model were the inflow conditions, weather conditions and bathymetry of the Tingalpa Reservoir. The model performed well in simulating the thermal structure and sediment-transport processes (Wang, Zhang, Bertone, Stewart, & O'Halloran, 2020). The outputs from the hydrodynamic and sediment-transport models were the inputs to the data-driven model. The data-driven model includes a turbidity-fDOM compensation model and a model further compensating fDOM for water temperature variations. The data-driven model can detect the change in dryness and wetness in the atmosphere and relate it to the current rainfall conditions, using the relevant equation. The following sections provide detailed information on the model. The structure of the coupled data-driven and process-based

model is shown in Figure 3. As shown in Figure 3, the models include a 3D hydrodynamic and sediment transport model and a data-driven model. Section 3.3 gives detailed information about the data-driven model and Section 3.4 introduces the modelling process of the process-based model.

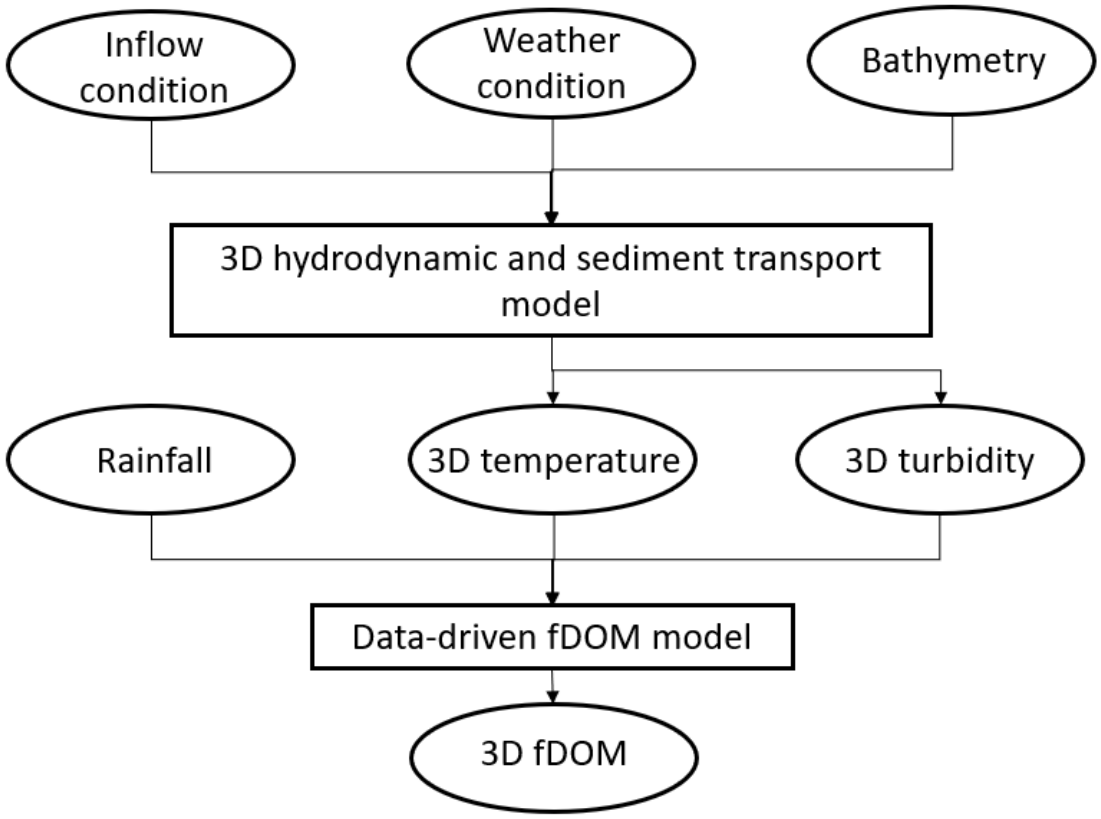

Figure 3. Coupled data-driven and process-based model structure.

4.2 Process-based model

The process-based model comprises a 3D time-dependent hydrodynamic model and a coupled sediment model. The numerical model, MIKE 3 FM (DHI, 2017), was applied to investigate the thermal structure and sediment transport process in the Tingalpa Reservoir. Wang et al. (2020) introduced the modelling process in detail and found that the process-based model simulates accurate water temperature and suspended sediment concentrations in three dimensions of the Tingalpa Reservoir. The output of the sediment model, the suspended sediment concentration, is the predictor for the turbidity concentration. The relationship between sediment concentration and turbidity varies at the different water depths at the VPS station. At a depth of 10 m, the relationship between sediment concentration and turbidity is divided into two cases: calm conditions and storm events. According to the data analysis, the minimum and maximum turbidity occurred at the depth

1 m and 10 m, especially during storms, and the turbidity shows a linear growth from the surface to bottom layers. So, these relationships between turbidity and sediment concentration were developed specifically at the depth of 1 m and 10 m. Eq. (1) gives the relationship between suspended sediment concentration and turbidity at a depth of 1 m during calm and storm conditions. Eq. (2) and Eq. (3) show the relationship between suspended sediment concentration and turbidity at a depth of 10 m during calm and storm conditions, respectively.

$$C_{t,1} = a_7 e^{b_7 C_{s,1}} \tag{1}$$

$$C_{t,10} = a_8 e^{b_8 C_{s,10}} + c_8 \tag{2}$$

$$C_{t,10} = a_8 e^{b_8 C_{s,10}} + c_8 + \Delta C_t \tag{3}$$

where $C_{t,1}$ is the turbidity concentration at a depth of 1 m [NTU], $C_{t,10}$ is the turbidity concentration at a depth of 10 m [NTU], $C_{s,1}$ is the suspended sediment concentration at a depth of 1 m [mg/L], $C_{s,10}$ is the suspended sediment concentration at a depth of 10 m [mg/L] and ΔC_t is the additional turbidity, which changes over time during storm events. We found factors $a_7 = 1.18$, $b_7 = 3.90\times10^{-1}$, $a_8 = 4.37$, $b_8 = 2.56\times10^{-1}$ and $c_8 = 9.00$. Eq. (2) is for the calm conditions and Eq. (3) is for the storm events. Figure 4 shows the time series ΔC_t during storm events.

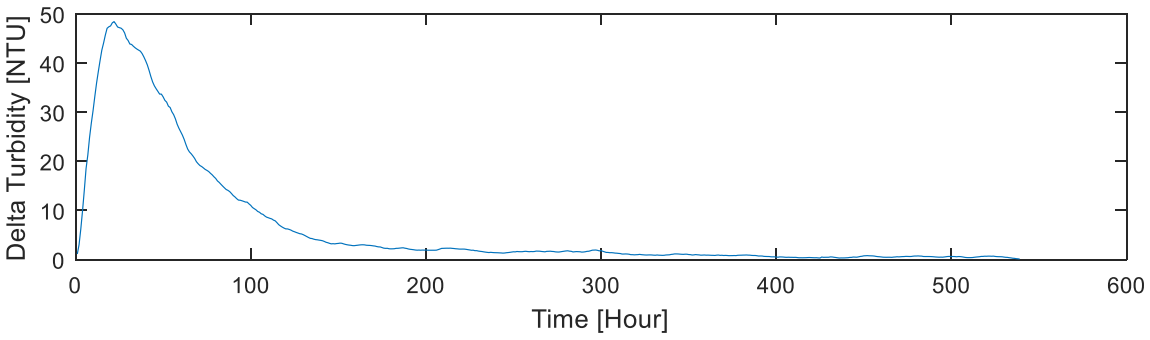

Figure 4. Time series of delta turbidity (NTU) during storm events at the depth of 10 m.

4.3 Data-driven model

Visually inspection was performed for the time-series graphs of all the related variables to determine whether the relationships described in the literature are confirmed in the real data from the Tingalpa Reservoir. When a relationship was identified, we performed a statistical analysis to quantify the correlation between variables.

The reading of fDOM is affected and distorted by turbidity, temperature, pH, salinity and inner filter effects. The type of turbidity, water temperature and the size of suspended particles are the decisive factors in the fDOM signal bias (Saraceno et al., 2017). Raw fDOM

probe measurements were validated as being more reliable if they were systematically compensated using the proposed procedure. The developed fDOM compensation procedure must consider the instrument features (i.e., wavelength broadband and responsiveness) and site-specific conditions (i.e., DOM characteristics and suspended particles). De Oliveira et al. (2018) developed a compensation model to investigate the turbidity and water temperature interferences in fDOM readings at the Tingalpa Reservoir. We applied such compensation model to obtain more reliable fDOM concentration under the influence of turbidity and the water temperature.

The compensated fDOM data at the VPS location confirmed that storm events could have led to peaks of compensated fDOM during the study period from June 2014 to March 2018. To investigate the compensated fDOM variance during storm events, we analysed each storm individually for the study period. There was a sharp increase in compensated fDOM from the original state, to a peak value, followed by continuous fluctuation and a final decrease to a compensated fDOM value that was higher than the value in the original state. Figure 5 shows the variance in compensated fDOM during one storm event and identifies several points. One storm event includes the compensated fDOM's growth period (T1) from the starting point to the critical point, a stable period (T2) from the critical point to the decrease starting point and the decline period (T3) from the decreasing starting point to an ending point.

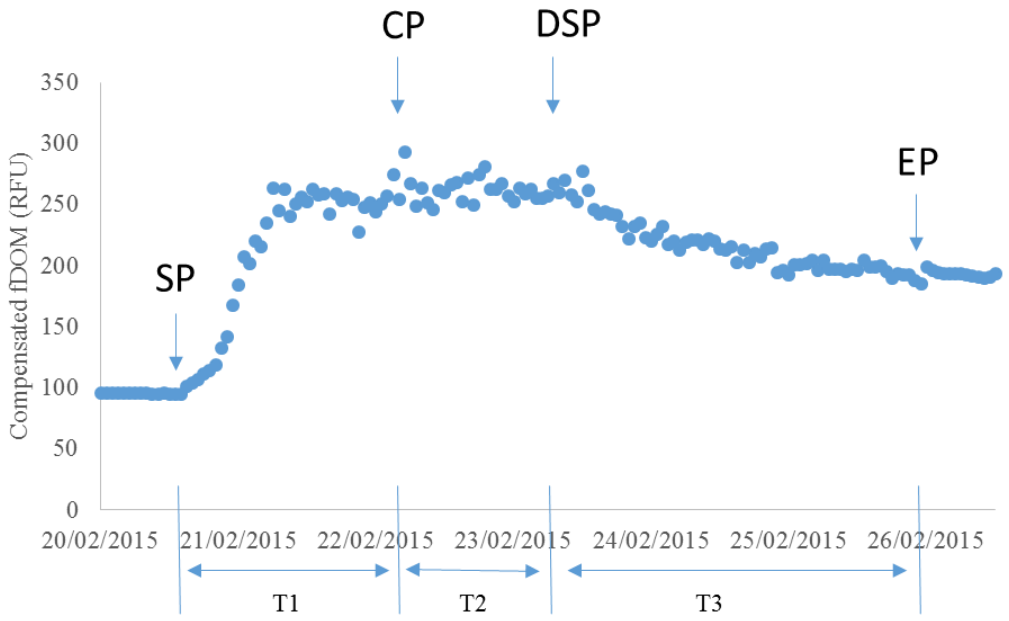

Figure 5. The time series of compensated fDOM (RFU) during a storm event. SP: starting point, CP: critical point, DSP: decrease starting point and EP: ending point. T1 is the compensated fDOM's growth period; T2 is the compensated fDOM's stable period; T3 is the compensated fDOM's decline period.

The moving average method was used to smooth the short-term fluctuation of compensated fDOM data, and a 10-h period was set to reduce lag by applying the weight to

recent compensated fDOM. In addition, the gradients of compensated fDOM during T1, T2 and T3 were calculated for 1 h. According to this analysis, the compensated fDOM's gradients were from 1.49 RFU/h to 11.51 RFU/h in the growth period at the depth of 10m, from 0 RFU/h to 1.26 RFU/h during the stable period and from 0.08 RFU/h to 4.52 RFU/h in the decline period. There is a specific search criterion to define heavy rainfall events. Identifying as heavy rainfall events any time there is the total rainfall over 50 mm in less than 2 days. Based on the available reliable data, there were five heavy rainfall events during the study period, and the time series of daily rainfall, turbidity and compensated fDOM for these five heavy rainfall events are shown in Figure 6.

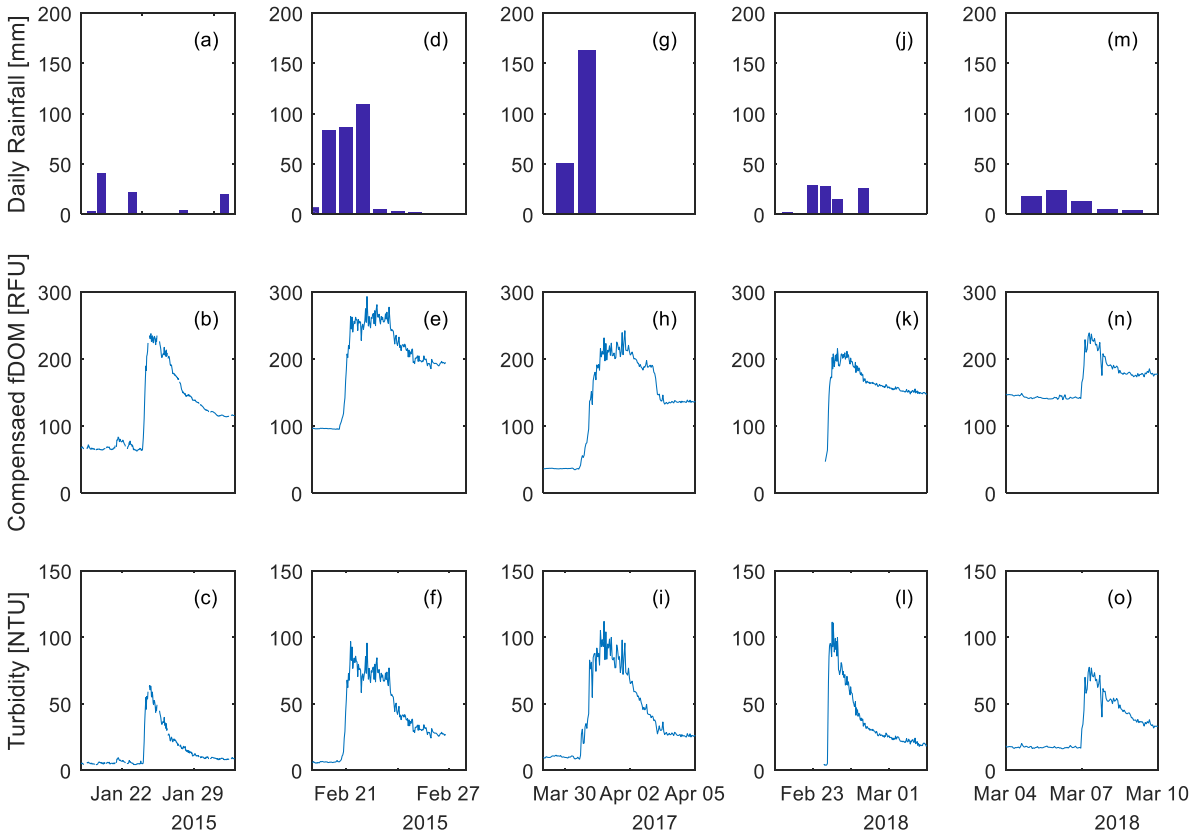

Figure 6. The time series of daily rainfall (mm), compensated fDOM (RFU) and turbidity (NTU) at a depth of 10 m at VPS station during Event 1 (a-c), Event 2 (d-f), Event 3 (g-i), Event 4 (j-l) and Event 5 (m-o).

Heavy rainfall increases the loading of sediments into the reservoir and accelerates the increase of sediment and turbidity. The high growth rate of turbidity results in a long lag between peak turbidity and peak fDOM concentration. In the Tingalpa Reservoir, the lag between peak turbidity and peak compensated fDOM was correlated with total rainfall during the storms, as shown in Figure 6a. Saraceno et al. (2009) found the lag time between peak turbidity and peak fDOM was 14 h at the mouth Willow Slough Watershed in Californa with a catchment area of 415 km^2, which is 4.7 times more than the catchment area of the Tingalpa Reservoir. The lag time and rainfall data in the study of Saraceno et al. (2009) are

shown as a reference in Figure 6a and these data agree with the correlation between total rainfall and lag time between peak turbidity and peak fDOM in the Tingalpa Reservoir. An analysis of the rainfall data and compensated fDOM data in Figure 6 found that the peak of compensated fDOM occurred during the period of intense rainfall during each storm event. For example, the intensive rainfall in Storm Event 2 occurred from 20 February to 23 February 2015, and the peak of fDOM occurred from 22 to 23 February 2015. Figure 7b shows the intensive rainfall during the prolonged peak period (T2) of compensated fDOM and the correlation between T2 and rainfall intensity. For the storm events with the same volume of rain, a high intensity means a short duration of rainfall. A short duration of rainfall also shortens the period of the fDOM's variance during the storm (T1 + T2 + T3). Their relationship between mean rainfall intensity and T1 + T2 + T3 is shown in Figure 7c. A high intensity of rainfall can accelerate the end of a storm and the decline period of fDOM (T3). A shortened T3 leads to a higher decrease in the gradients of compensated fDOM during T3. The correlation between this decrease in gradients and rainfall intensity is shown in Figure 7d. Figure 6 shows the relationships between parameters related to rainfall and those related to the changes in compensated fDOM at a depth of 10m at the VPS station during five storm events.

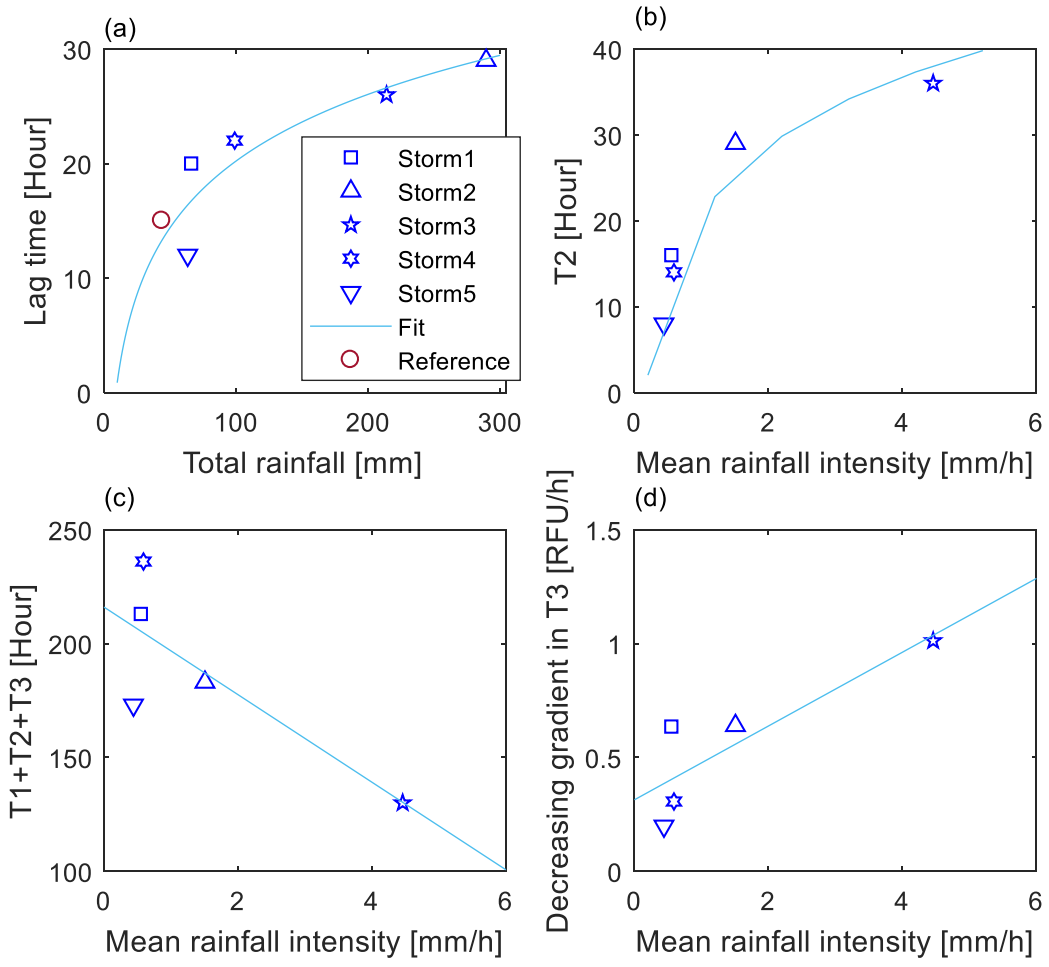

Figure 7. Scatter plot and regression between parameters related to rainfall and parameters related to the changes of compensated fDOM at a depth of 10 m during five major storm events. (a) relationship between total rainfall and lag from peak turbidity to peak compensated fDOM and the reference data from Saraceno et al. (2009); (b) relationship between mean rainfall intensity and the duration of the stable period of compensated fDOM (T2); (c) relationship between mean rainfall intensity and T1 + T2 + T3 and (d) relationship between mean rainfall intensity and compensated fDOM decreasing gradient.

Plotting the compensated fDOM values against all possible predictors showed which type of nonlinearity links the variables. The most relevant results to our study are shown in Figure 8, representing a clear parabolic correlation between turbidity and compensated fDOM data from the growth periods and stable periods of fDOM variances during the storm events. We expected these results because of the delayed fluorescence response of fDOM during storms compared to the turbidity found in the literature and confirmed in the Tingalpa Reservoir. Figure 8a shows that the fDOM difference (the difference value of compensated fDOM, when turbidity equals zero) high for the second and third storm events and resulted from intense rainfall during these storms. The lower part of the parabolic correlation represents the compensated fDOM's during its increasing pattern during the period when the turbidity increases, whilst the upper part, above the vertex, is representative of the compensated fDOM's increasing part during the lag time between peak turbidity and peak fDOM. The vertex of the parabolic correlation represents the compensated fDOM when the turbidity reaches the peak value.

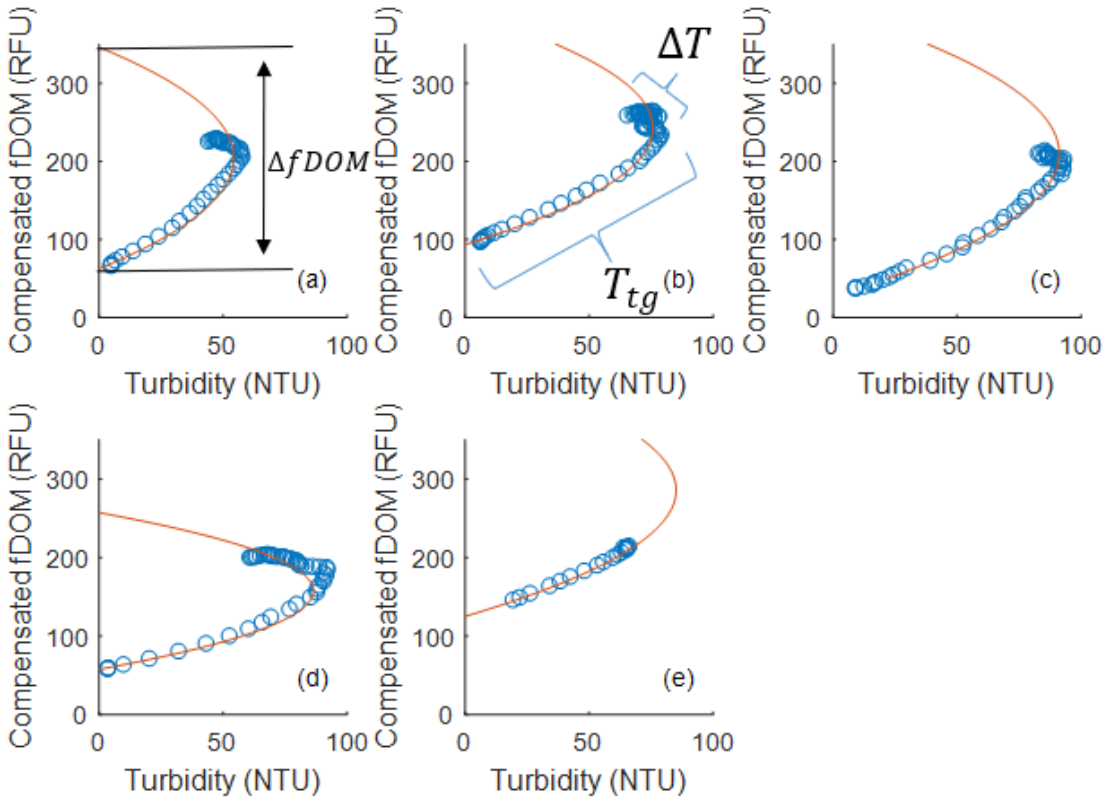

Figure 8. Scatter plot of compensated fDOM (RFU) and turbidity (NTU) at a depth of 10 m for (a) Storm Event 1 (ΔfDOM represents the fDOM difference in the regression between turbidity and compensated fDOM), (b)

Storm Event 2, (c) Storm Event 3, (d) Storm Event 4 and (e) Storm Event 5, the lower part of the parabolic correlation represents the part of the storm event in the increasing period of turbidity (Ttg) and the upper part of the parabolic correlation represents the part of the storm event during the lag time between peak turbidity and peak compensated fDOM (ΔT).

When the statistical analysis was complete and the features and correlations of the data were identified, it was possible to derive the most appropriate model and its key input parameters, shown in Figure 9. The data-driven model consisted of two parts to ensure accurate and reliable compensated fDOM prediction. The second model part needed to be further divided into two parts.

The three model parts are as follows:

- **Model Part 1**: This part includes a determination of whether the heavy rainfall leads to the compensated fDOM increase and the prediction of one storm period (T1 + T2 + T3). To determine whether the heavy rainfall caused the increase of compensated fDOM, two requirements need to be satisfied: 1.the total rainfall in two days is more than 50 mm and 2. gradients of the simulated turbidity from the process-based model in these two days are more than 0.80 NTU/h. One storm event period for compensated fDOM includes T1, T2 and T3. T1, T2 and T3 are predicted based on Eq. (4), Eq. (5), Eq. (5) and Eq. (9). If the studied period is not in the storm event period, it belongs to the calm conditions.
- **Model Part 2.1**: This part takes the turbidity outputs in the calm category. Using the consistent decreasing rate, it yields a prediction of the fDOM in calm conditions.
- **Model Part 2.2**: This part takes the turbidity outputs from Part 1 in the storming category. Using the parabolic correlation between turbidity and compensated fDOM, the compensated fDOM under turbidity's effect predicted in T_{tg} and ΔT during storm events, shown in Figure 8. The prediction of compensated fDOM in T1, T2 and T3 based on the Eq. (6), Eq. (7) and Eq. (10).

All models must be validated. In most time-series forecasting studies, this is usually achieved by dividing the dataset into a training set and a testing set, where the model is built, and the performance of the model is assessed. During this study, the Tingalpa Reservoir experienced five storm events during the monitoring period. Therefore, the training set contains the first to the fourth storm events from Model Part 2.2. The fifth storm belongs to the testing set to validate the model's accuracy.

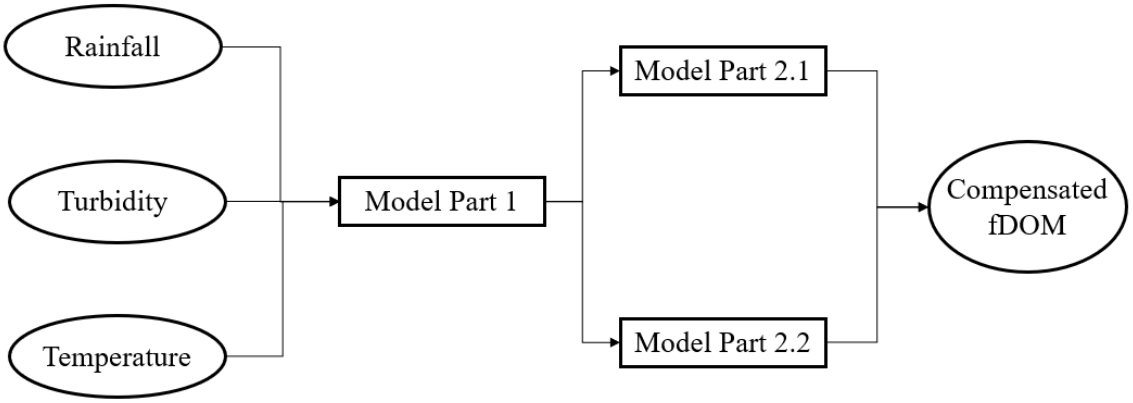

Figure 9. Integrated data-driven model structure.

Model part 2.2 can simulate the compensated fDOM's periods of growth, stability and decline. The model was calibrated using the training set of data (i.e., Storm Events 1 - 4) and performance was tested on the testing set (i.e., Storm Event 5) for Model Part 2.2. The compensated fDOM's growth period is regarded as the total period of the turbidity's growth and the lag between peak turbidity and peak compensated fDOM, given by Eq. (4). The lag between peak turbidity and peak fDOM relates to the rainfall, following Eq. (5):

$$T_1 = T_{tg} + \Delta T \tag{4}$$

$$\Delta T = a_1\, ln(R) + b_1 \tag{5}$$

where T_1 is the compensated fDOM's growth period [hour], T_{tg} is the turbidity's growth period [hour] and ΔT is the lag between peak turbidity and peak compensated fDOM [hour], R represents the rainfall amount [mm] during this storm event. It was found that the best logarithmic regression is based on factors a_1 = 8.40 and b_1 = -1.85×10^1 with a correlation coefficient for the test set of 0.85.

During the compensated fDOM's growth period, the parabolic regression between compensated fDOM and turbidity was accounted for. Eq. (6) describes the relationship between turbidity and compensated fDOM:

$$f = \frac{\pm\sqrt{{b_2}^2 - 4a_2c_2 + 4a_2C_t} - b_2}{2a_2} \tag{6}$$

where f is the compensated fDOM concentration [RFU] and C_t is the turbidity concentrations [NTU]. During the period T_{tg}, the "-" solution is calculated to get the

compensated fDOM concentration and the "+" solution is used during the period ΔT. The coefficients a_2, b_2 and c_2 determine the fDOM difference [RFU], shown in Figure 8a. The fDOM difference varied by storm and water depth. The relation between the fDOM difference for the different water depths and storm events was found using Eq. (7).

$$\Delta fDOM = (a_3 \frac{R}{T_R} + b_3)z + c_3 R + d_3 \quad (7)$$

where $\Delta fDOM$ represents the fDOM difference in the regression between the turbidity and compensated fDOM, T_R is the rainfall duration [hour] for one storm event and z being the water depth [m]. We found factors $a_3 = 6.57$, $b_3 = 1.83\times10^1$, $c_3 = -2.34\times10^{-1}$, $d_3 = 1.52\times10^2$, and the coefficient determination (R^2) = 0.79 for the test set. According to the data analysis, a logarithmic regression was found between rainfall duration and stable period, using Eq. (8). During the stable period, fDOM remained at the fDOM peak level.

$$T_2 = a_4 ln\,(\frac{R}{T_R}) + b_4 \quad (8)$$

where T_2 is the duration of the compensated fDOM's stable period [hour]. We found factors $a_4 = 1.16\times10^1$ and $b_4 = 2.07\times10^1$, and $R^2 = 0.91$ for the test set.

We found a correlation between the duration of compensated fDOM period and rainfall intensity. We tested the linear regression model between rainfall intensity and total fDOM period. We found factors $a_5 = -1.92\times10^1$, $b_5 = 2.16\times10^2$ and $R^2 = 0.68$ for the test set, using Eq. (9). During the compensated fDOM's decline period, we found a stable decline rate. Using Eq. (10), we calculated the linear regression between rainfall intensity and the compensated fDOM's mean decrease rate. Eq. (10) was applied to predict the compensated fDOM concentration gradient during the fDOM's decline period.

$$T_1 + T_2 + T_3 = a_5 \frac{R}{T_R} + b_5 \quad (9)$$

$$g_d = a_6 \frac{R}{T_R} + b_6 \quad (10)$$

where T_2 is the compensated fDOM's stable period [hour], T_3 is the compensated fDOM's decline period [hour] and g_d is the compensated fDOM's mean gradient during the decline period. Using Eq. (10), we found $a_6 = 1.62\times10^{-1}$, $b_6 = 3.14\times10^{-1}$ and $R^2 = 0.80$ for the test set.

4.4 Model validation

Figure 10 shows the time series of turbidity from measurements and from the process-based model for the storm events from 30 Apr to 10 May 2015 at the VPS station. The root mean square error for the depths of 1 m and 10 m were 3.61 and 3.83 NTU, respectively. The coefficients of determination were 0.91 and 0.87 at the depth of 1 m and 10 m during this storm as a test set. Figure 10 shows that the main peak was accurately simulated during the storms in the model. The simulation of turbidity at the depths of 1 m and 10 m is a robust validation of the process-based model. It can be adapted to evolving extreme storm events in reservoirs.

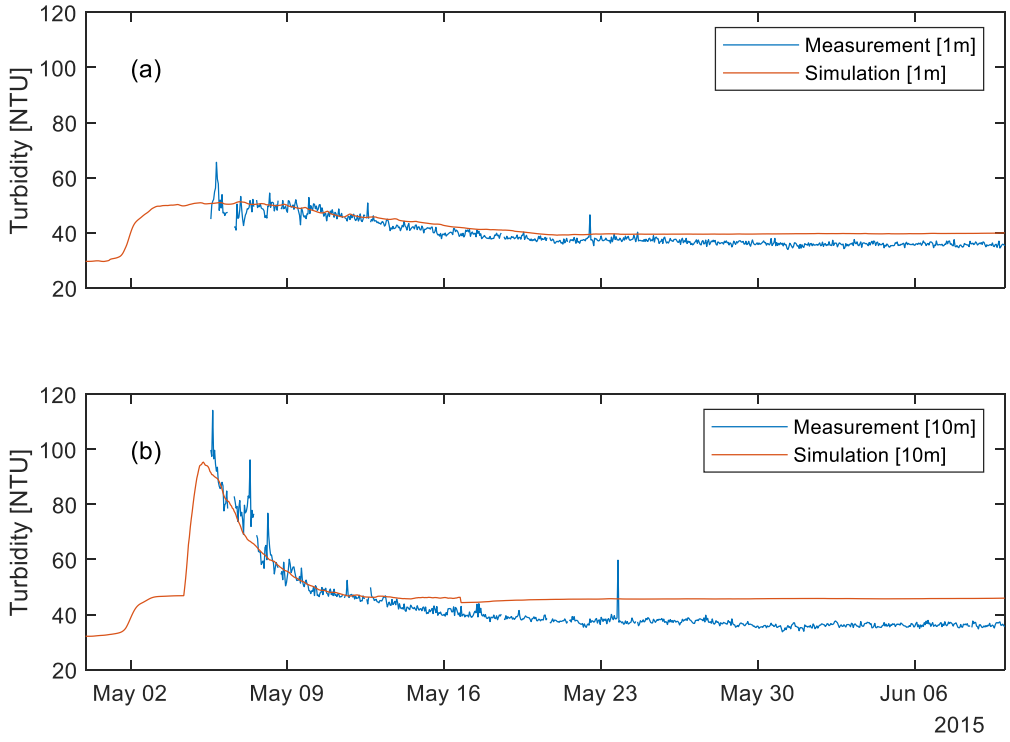

Figure 10. A comparison of measurement and simulation of turbidity from May to Jun 2015 at (a) a depth of 1 m and (b) a depth of 10 m.

Figure 11 shows the time series of simulated and measured compensated fDOM during the storm events from April to June 2015 at the VPS station. The root mean square error for the depths of 1 m and 10 m were 2.65 RFU and 2.78 RFU, respectively. The coefficients of determination achieved for compensated fDOM were 0.92 and 0.97 at the depths of 1 m and 10 m, respectively. The simulation was accurate. Overall, the coupled data-driven and process-based model can accurately predict the fDOM concentration in the water column during a storm.

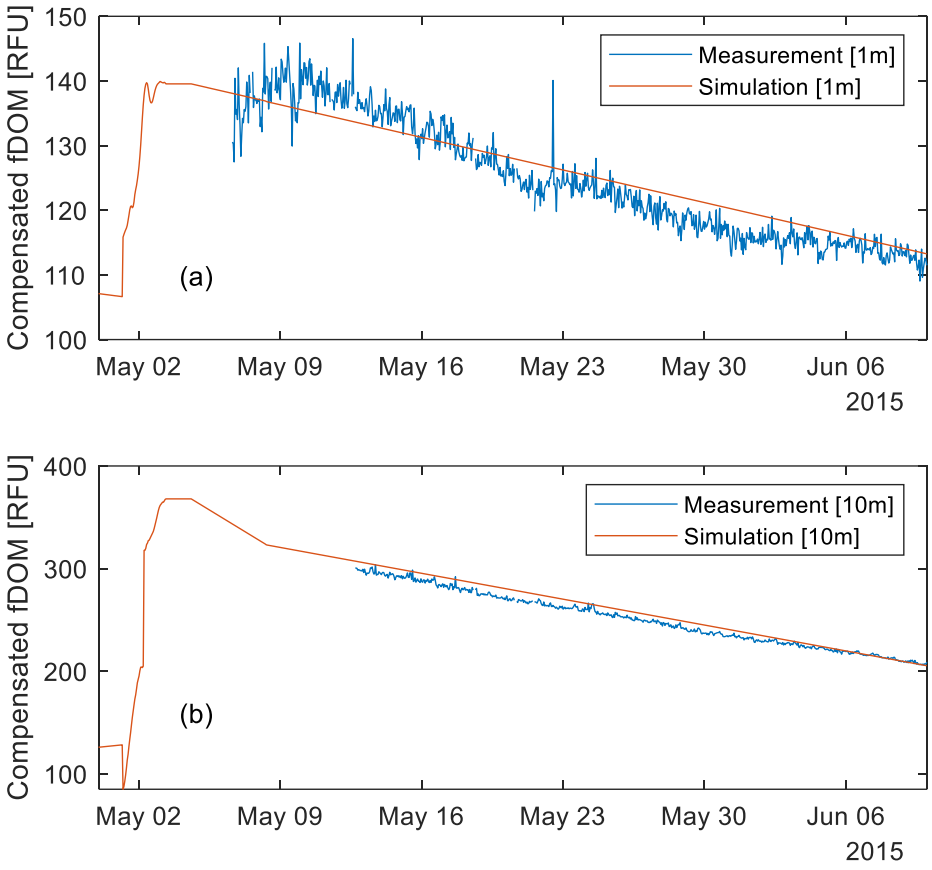

Figure 11. A comparison of measurement and simulation of compensated fDOM from May to Jun 2015 at (a) a depth of 1 m and (b) a depth of 10 m.

As part of a recent investigation by our group (De Oliveira et al., 2018), a number of samples from Tingalpa were collected in May–September 2017; laboratory work, including dilution series, enabled the creation of a dataset where a correlation between compensated fDOM and DOC could be established. According to the data analysis of our water sampling, the measured data show there is a correlation between compensated fDOM and DOC concentration in the Tingalpa Reservoir. The DOC concentration is given by Eq. (11).

$$DOC = a_9 ln\,(fDOM) + b_9 \tag{11}$$

where *DOC* is the DOC concentration [mg/L] and *fDOM* is the compensated fDOM concentration [RFU]. We found factors a_9 = 6.30 and b_9 = -1.10×10^1, and R^2 = 0.89 for the test set. The correlation was applied to validate the modelled fDOM, and the DOC concentration was simulated at an hourly interval. Comparisons between measured and simulated DOC concentrations are shown in Figure 12 at SP001, SP002, SP004, SP010 and SP015. Compared to the measured DOC, the simulated data at each respective time

point had the same range as the measured data from 0 to 20 mg/L. The simulated DOC concentration over 20 mg/L occurred during storms at the bottom layer of the reservoir. Because the DOC data was monitored before the storm event, the concentration lower than 20 mg/L. Overall, the coupled data-driven and process-based model can accurately predict the fDOM concentration in a water column during a storm.

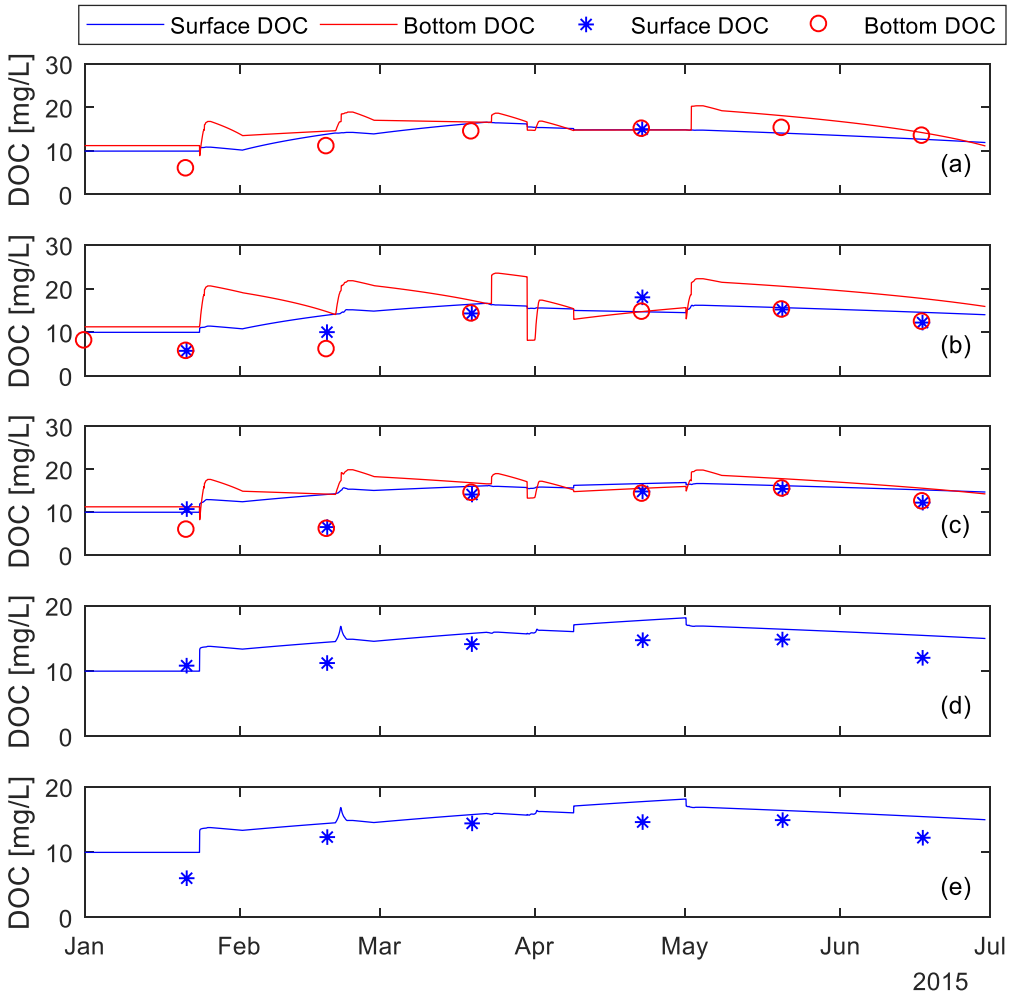

Figure 12. Simulated and measured DOC concentrations at the surface and bottom layers of the reservoir at (a) SP001, (b) SP002, (c) SP004, (d) SP010 and (e) SP015.

5. Results and discussion

To establish the effects of storms on the reservoir, the simulated fDOM and measured DOC concentrations were plotted from January 2015 to July 2015. Figure 13 shows the simulation of fDOM and measurement of DOC at SP001, SP002, SP004, SP010 and SP015. SP001, SP002 and SP004 are in the north west, west and east of the reservoir, respectively, shown in Figure 1. Figure 13 shows that the water depths at SP001, SP002 and SP004 are 3 m, 10 m and 5 m, respectively. SP010 and SP015 belong to the riverine zone, and these stations are close to the inflow creeks. Due to the shallow water depth at the riverine zone, the DOC concentration was measured only at the surface layer of the water. Due to the

monthly monitoring interval for the DOC concentration, only the rough variance of DOC could be analysed. The DOC concentration at the surface had the same variance in the first half of 2015. It increased from January, reached its peak value in May and then decreased. The simulated fDOM at the top layer of the reservoir at five monitored stations also had the same variance as the surface DOC concentration. The simulated fDOM at the surface increased from January, reached its highest level in April and May and then declined. Compared to the lacustrine zone, the riverine zone's surface DOC at SP010 and SP015 had a sharper increase during the storm in February 2015. This increase resulted from inflow creeks with high turbidity during the storm event. Simulated bottom fDOM at three stations clearly fluctuated, especially during storms. Due to the deepest point at SP002 station, the peak values of bottom fDOM at SP002 during storms were the highest than other stations. Overall, the simulated surface and bottom fDOM from the coupled data-driven and process-based model showed the temporal and spatial variances in the Tingalpa reservoir. The fDOM variances can be a proxy for DOC concentration changes during wet weather events.

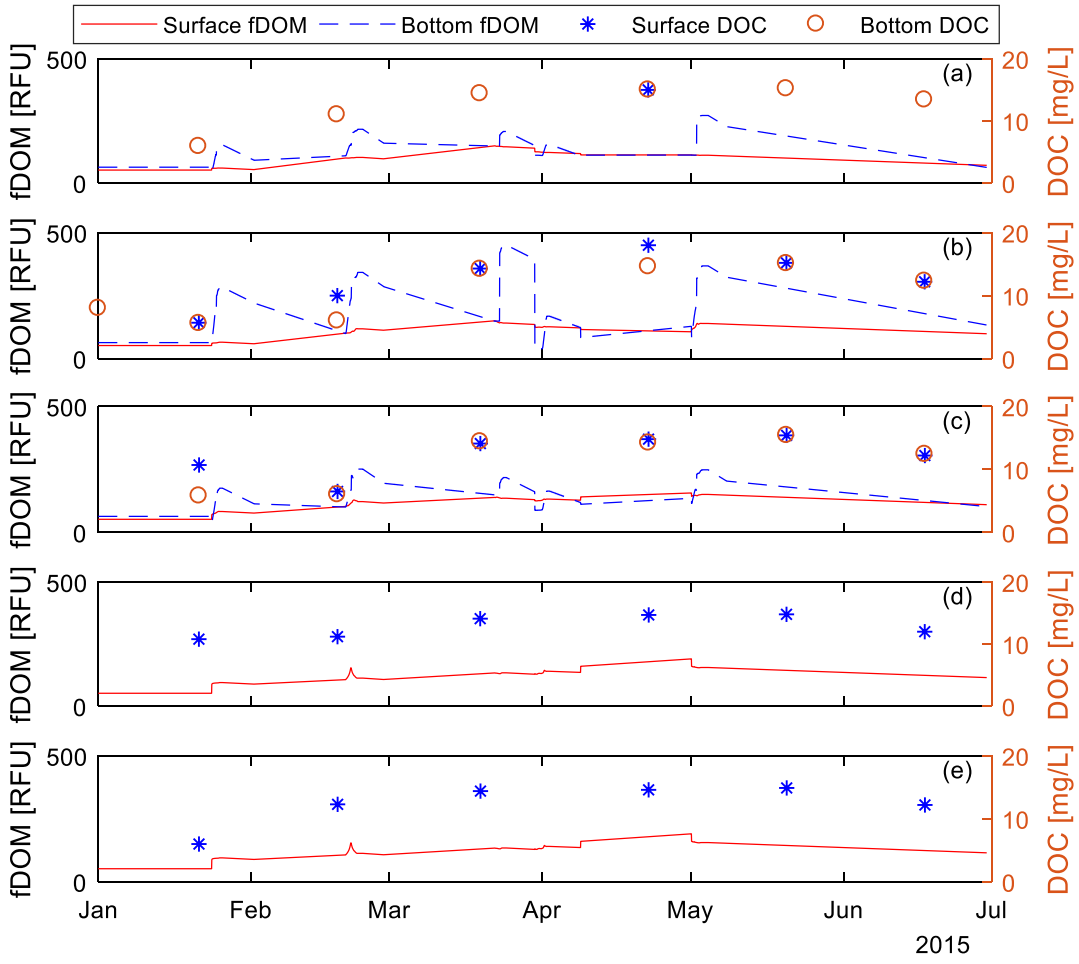

Figure 13. Time series of simulated fDOM and measured DOC at top and bottom layers of the Tingalpa Reservoir at the (a) SP001, (b) SP002, (c) SP004, (d) SP010 and (e) SP015, January to July 2015, Lake Tingalpa.

To analyse the influence of the storms on the fDOM transport, the compensated fDOM at the surface layer of the reservoir was predicted before, during and after the February storm with high rainfall intensity in 2015. As displayed in Figure 14a, the overall horizontal fDOM was below 110 RFU before the storm. Figure 14b indicates that the inflow water with high fDOM led to an increase of DOM, especially in the area close to the inflow creeks. The plume contained a high concentration of fDOM spread to the centre of the lake during the storm and because of dilution, the water with fDOM higher than 150 RFU did not transport to a long distance. Figure 14d reveals that there was an obvious increase of fDOM in the east and west branches of the lake after the storm. Therefore, as illustrated in Figure 14, the variation of surface fDOM distribution mainly depends on the high concentration of fDOM in the inflow plume.

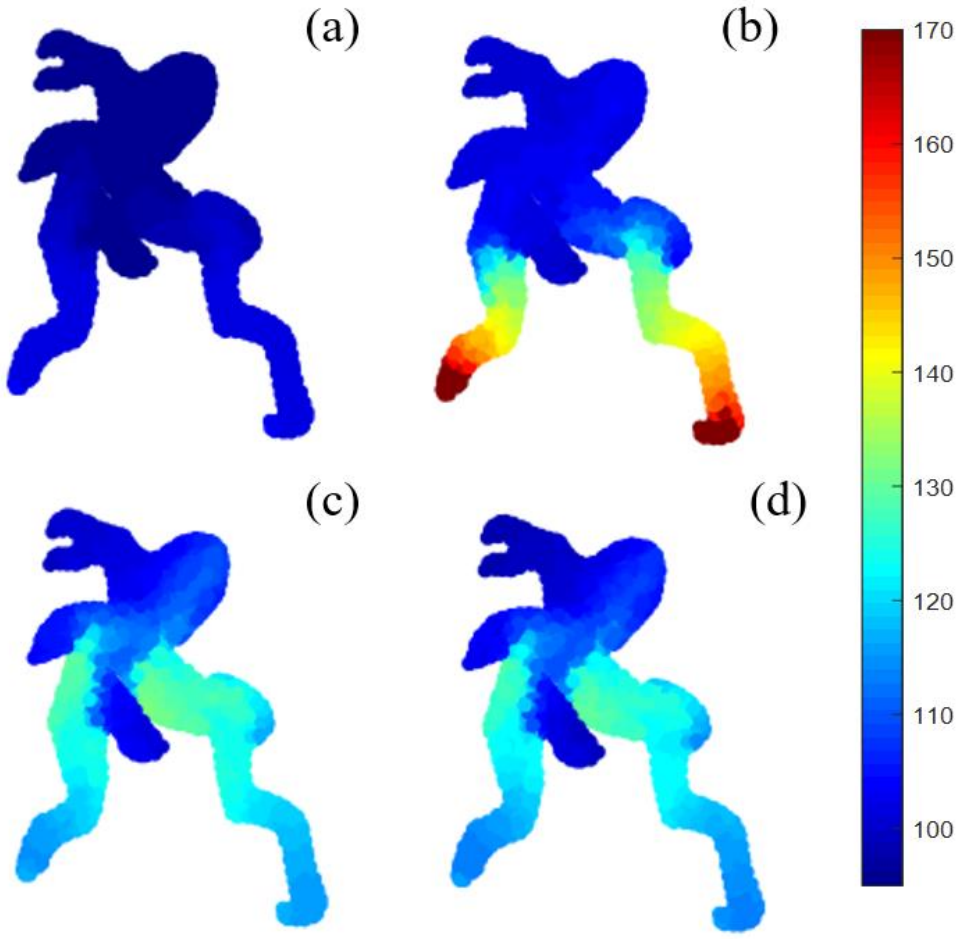

Figure 14. The simulated horizontal distribution of the surface compensated fDOM during Cyclone Marcia in the Tingalpa Reservoir on (a) 18th, (b) 21st, (c) 22nd and (d) 24th of February 2015; the color legend represents the compensated fDOM (RFU).

The time series of the rainfall amount, water level and simulated compensated fDOM at the depth of 3 m in the riverine, transition and lacustrine zones are displayed in Figure 15. The meteorological characteristics and simulated results during the main storm events are

shown in Table 2. As depicted in Figure 15, the heavy rainfall led to an increase in both water level and simulated fDOM. Figure 15b demonstrates that the fDOM at the depth of 3m in riverine firstly reached the peak during the storm. As shown in Table 2, these five storms were primarily caused by heavy rainfall and when the rainfall intensity was higher than 2.3 mm/h, the peak fDOM in the lacustrine zone was greater than 161.6 RFU. Moreover, the lag time between the start of the rainfall and peak fDOM was longer in the first storm event. The observation can be explained by lower rainfall intensity and no storm event occurred before the storm event 1, so there was a long time for fDOM to react to the heavy rainfall. Figure 15 shows the lag time that existed between peak fDOM in the riverine zone and lacustrine zone. The lag time between peak fDOM in the riverine zone and lacustrine zone were from 16 h to 90 h during these events. The lag time between peak fDOM in the riverine zone and the lacustrine zone is the shortest in Event 4, this can be explained by the short interval from Event 3 to Event 4, which also led to a lowest concentration of peak fDOM. Except the Event 4, the peak of fDOM in the lacustrine zone was higher than 100 RFU. The higher concentration of fDOM indicates that the storm event led to the DOM's increase, which needs more attention to remove extra DOM in water treatment. The simulation results implicate that the water treatment needs to have 34 h to respond once a peak of fDOM is recorded in the riverine zone.

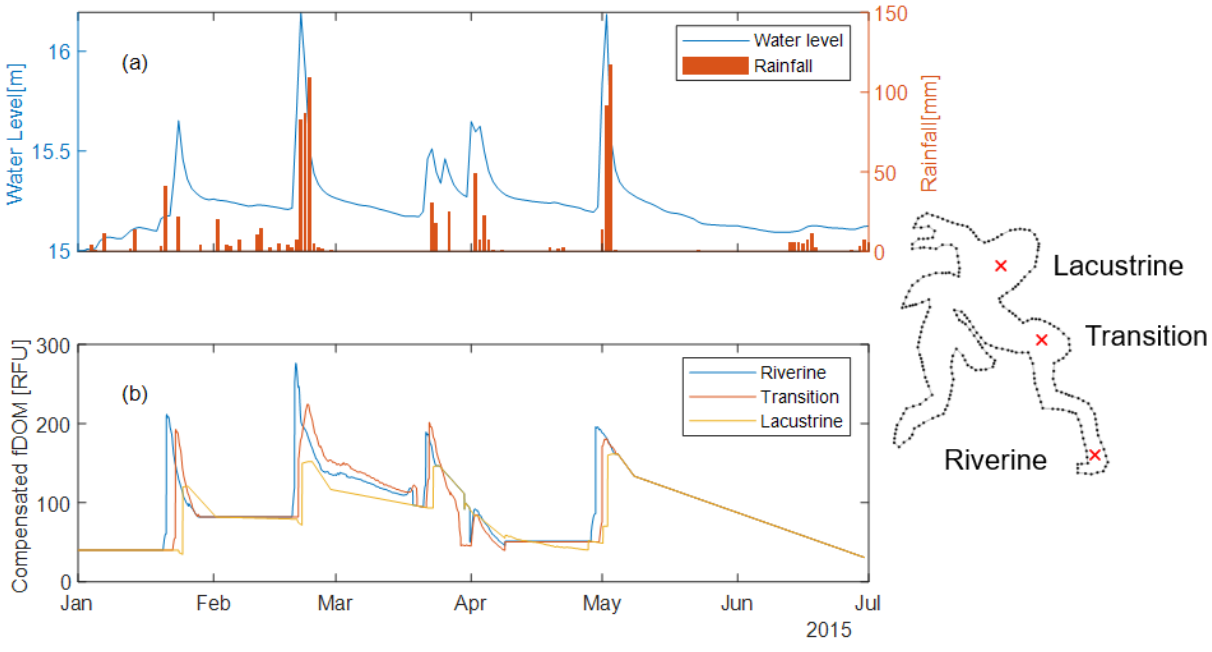

Figure 15. The time series of (a) surface elevation (m) and rainfall (mm) and (b) simulated compensated fDOM (RFU) at the riverine, transition and lacustrine zones at the depth of 3 m January - July 2015.

Table 2. The meteorological characteristics of the storm events and the relevant simulated results during study period.

Parameter	Event 1	Event 2	Event 3	Event 4	Event 5
Time period	19/01/2015-29/01/2015	20/02/2015-26/02/2015	22/03/2015-27/03/2015	02/04/2015-08/04/2015	30/04/2015-03/05/2015
Rainfall magnitude (mm)	66.6	288.8	74.4	89.0	223.4
Storm duration (h)	216	120	96	168	94
Rainfall intensity (mm/h)	0.31	2.41	0.78	0.53	2.38
Peak fDOM in the lacustrine zone (RFU)	119.4	151.7	145.2	76.0	161.6
Lag time from the start time of rainfall to the peak fDOM in the lacustrine zone (hr)	134	79	26	11	56
Lag time between peak fDOM in riverine zone and peak fDOM in the lacustrine zone (hr)	90	34	41	16	49

To indicate the fDOM variation under wind conditions, the simulated horizontal and vertical distributions of compensated fDOM under west wind were analysed. The continuous west wind blew from 10 a.m. to 2 p.m. on 22 May 2015 with the wind speed varying from 1 m/s to 6.6 m/s. The simulated lake-wide circulation pattern at the top and bottom layers of the water column is shown in Figure 16. It is found the currents at the surface centre of the lake flowed to the east, same as the wind direction and the currents at the bottom of the centre lake flowed to the west. The flow directions at the surface and bottom layers of the lake were opposite, which suggests there was a transport cycle present in the vertical direction of the lake. The simulated results show that the fDOM at the surface was lower than the bottom of the lake. The water cycle in the vertical direction under continuing west winds is the main factor that caused the higher fDOM concentration in west areas of the lake than east areas at the deep layer of the lake.

Figure 17 presents the vertical distribution of the simulated fDOM from IP1 to IP2 on 22 May 2015. For the flow direction, the currents at the surface water to the depth of 2 m had the same direction as the wind, and the water below the depth of 2 m flowed in the reverse direction. It is found that the water column near IP1 flowed up and the water near IP2 flowed down. Moreover, the water column at the middle between IP1 and IP2 flowed to the surface

layers of the lake, due to the terrain of the reservoir; in other words, when water flows to the shallow area, it will lead to the upward or downward water flow. It is obvious that the fDOM near IP1 was higher than that near IP2 at the depth of 5 m and 6 m, this phenomenon indicates that the water cycle in the vertical direction transported the fDOM from bottom layers to the top layers of the lake.

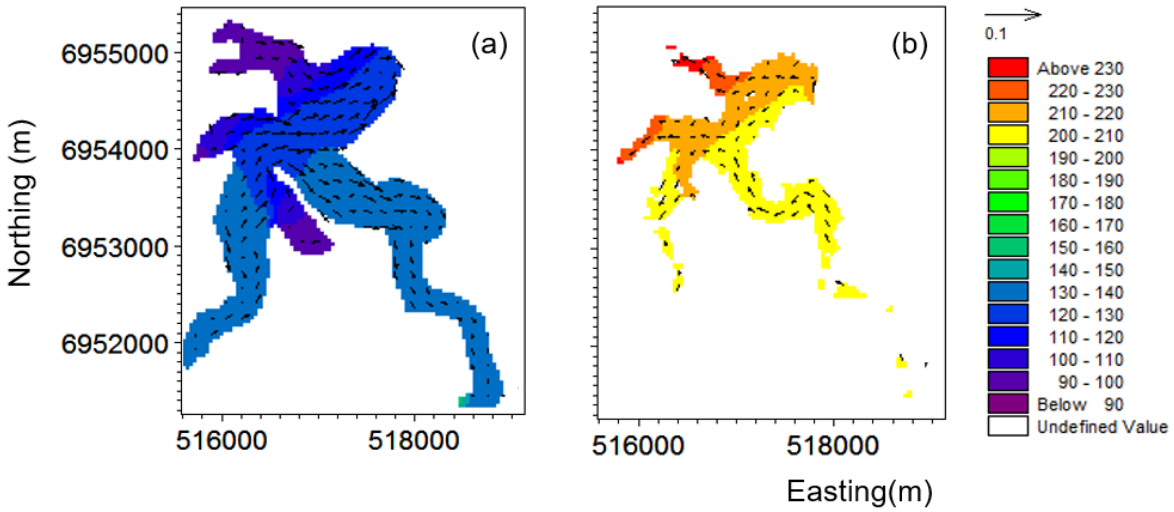

Figure 16. (a) Simulated top cell-averaged velocity and simulated compensated fDOM (10 a.m. to 2 p.m.) on 22 May 2015 and (b) the simulated bottom cell-average velocity and simulated compensated fDOM (10 a.m. to 2 p.m.) on 22 May 2015; the vectors represent the flow velocity.

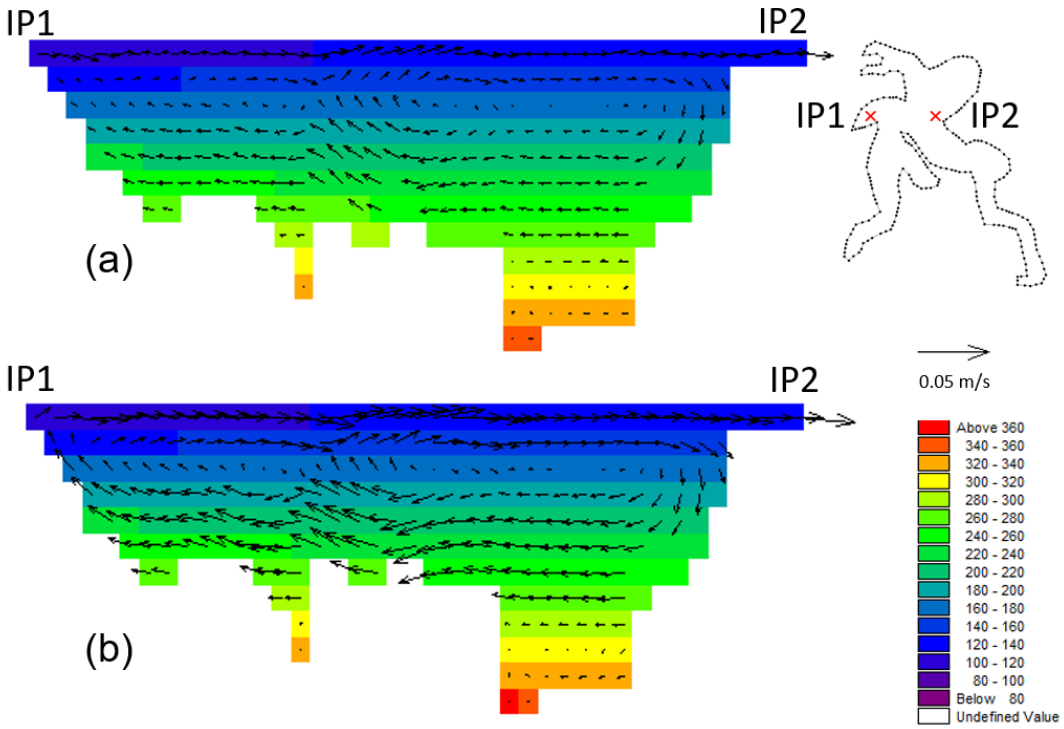

Figure 17. (a) The simulated vertical distribution of compensated fDOM at 10 a.m. on 22 May 2015 and (b) the simulated vertical distribution of compensated fDOM at 2 p.m. on 22 May 2015; the color legend represents the compensated fDOM (RFU).

6. Conclusion

This study has investigated the cycle of fDOM in lakes and reservoirs and explored the relationships between fDOM and relevant parameters, including turbidity, rainfall and water temperature. A coupled data-driven and process-based model was developed and validated using collected data during storm events and calm conditions. The model showed accuracy in replicating the observed variations of fDOM and reproduced the magnitude and distribution of turbidity. The simulated results indicate that deeper layers of the reservoir had higher fDOM concentrations during storms, and the area close to the riverine zone had a sharper increase during storm events. The simulated fDOM can be a proxy of DOC concentration. The simulation results indicate that the increase of fDOM during the storm at the surface of the lake was mainly caused by the inflow plume, in other words, fDOM sources were from inflow creeks. The model results show the lag times between peak fDOM in the riverine zone and lacustrine zone are from 16 h to 90 h during the studied period. To remove the DOM efficiently, the water treatment needs to have 34 h to respond once a peak of fDOM is recorded in the riverine zone. The analysis of wind influence on fDOM transport was also conducted. It was found that the continuing wind caused the water cycle in the vertical direction and led to the transport of fDOM from the bottom layers to the surface layer of the reservoir. The fDOM prediction model developed in this study provides an innovative method to simulate the three-dimensional fDOM dynamics in reservoirs. This innovative model will help water treatment operators to manage and improve the quality of the water sources, especially to remove DOM.

Acknowledgements: The authors would like to acknowledge DHI Water and Environment, Denmark, for their assistance in providing MIKE modelling system for this study. This research work was conducted with the technical support of Griffith University and Seqwater. The authors would like to acknowledge Jonathan Creamer for technical advice.

Author Contributions: Conceptualization, X.W., H.Z., E.B. and R.S.; methodology, X.W. and H.Z.; software, X.W.; validation, X.W. and E.B.; formal analysis, X.W.; data curation, S.H.; writing—original draft preparation, X.W.; writing—review and editing, H.Z., E.B., R.S. and S.H..

Conflicts of Interest: The authors declare no conflict of interest.

Uncategorized References

Ask, J., Karlsson, J., Persson, L., Ask, P., Byström, P., & Jansson, M. (2009). Terrestrial organic matter and light penetration: Effects on bacterial and primary production in lakes. *Limnology and oceanography, 54*(6), 2034-2040.

Awad, J., van Leeuwen, J., Chow, C., Drikas, M., Smernik, R. J., Chittleborough, D. J., & Bestland, E. (2016). Characterization of dissolved organic matter for prediction of trihalomethane formation potential in surface and sub-surface waters. *Journal of hazardous materials, 308*, 430-439.

Bergamaschi, B. A., Krabbenhoft, D. P., Aiken, G. R., Patino, E., Rumbold, D. G., & Orem, W. H. (2012). Tidally driven export of dissolved organic carbon, total mercury, and methylmercury from a mangrove-dominated estuary. *Environmental Science & Technology, 46*(3), 1371-1378.

Bertuzzo, E., Helton, A. M., Hall Jr, R. O., & Battin, T. J. (2017). Scaling of dissolved organic carbon removal in river networks. *Advances in Water Resources, 110*, 136-146.

Carstea, E. M. (2012). Fluorescence spectroscopy as a potential tool for in-situ monitoring of dissolved organic matter in surface water systems. In *Water pollution*: InTech.

Carstea, E. M., Popa, C. L., Baker, A., & Bridgeman, J. (2019). In situ fluorescence measurements of dissolved organic matter: A review. *Science of the Total Environment*, 134361.

Coble, P. G. (1996). Characterization of marine and terrestrial DOM in seawater using excitation-emission matrix spectroscopy. *Marine Chemistry, 51*(4), 325-346.

Cyr, F., Tedetti, M., Besson, F., Beguery, L., Doglioli, A. M., Petrenko, A. A., & Goutx, M. (2017). A new glider-compatible optical sensor for dissolved organic matter measurements: test case from the NW Mediterranean Sea. *Frontiers in Marine Science, 4*, 89.

De Oliveira, G. F., Bertone, E., Stewart, R. A., Awad, J., Holland, A., O'Halloran, K., & Bird, S. (2018). Multi-parameter compensation method for accurate in situ fluorescent dissolved organic matter monitoring and properties characterization. *Water, 10*(9), 1146.

DHI. (2017). MIKE 3 Flow Model, Hydrodynamic Module, Scientific Documentation. DHI Water & Environment, Horsholm.

Downing, B. D., Pellerin, B. A., Bergamaschi, B. A., Saraceno, J. F., & Kraus, T. E. (2012). Seeing the light: The effects of particles, dissolved materials, and temperature on in situ measurements of DOM fluorescence in rivers and streams. *Limnology and Oceanography: Methods, 10*(10), 767-775.

Druon, J., Mannino, A., Signorini, S., McClain, C., Friedrichs, M., Wilkin, J., & Fennel, K. (2010). Modeling the dynamics and export of dissolved organic matter in the Northeastern US continental shelf. *Estuarine, Coastal and Shelf Science, 88*(4), 488-507.

Dubinsky, Z., & Rotem, J. (1974). Relations between algal populations and the pH of their media. *Oecologia, 16*(1), 53-60.

Fabris, R., Chow, C. W., Drikas, M., & Eikebrokk, B. (2008). Comparison of NOM character in selected Australian and Norwegian drinking waters. *Water Research, 42*(15), 4188-4196.

Gjessing, E. T. (1976). Physical and chemical characteristics of aquatic humus.

Henderson, R. K., Baker, A., Murphy, K., Hambly, A., Stuetz, R., & Khan, S. (2009). Fluorescence as a potential monitoring tool for recycled water systems: a review. *Water Research, 43*(4), 863-881.

Holland, A., Stauber, J., Wood, C. M., Trenfield, M., & Jolley, D. F. (2018). Dissolved organic matter signatures vary between naturally acidic, circumneutral and groundwater-fed freshwaters in Australia. *Water Research, 137*, 184-192. doi:https://doi.org/10.1016/j.watres.2018.02.043

Huber, S. A. (1998). Evidence for membrane fouling by specific TOC constituents. *Desalination, 119*(1-3), 229-234.

Hudson, N., Baker, A., & Reynolds, D. (2007). Fluorescence analysis of dissolved organic matter in natural, waste and polluted waters—a review. *River Research and Applications, 23*(6), 631-649. doi:10.1002/rra.1005

Jack, J., Sellers, T., & Bukaveckas, P. A. (2002). Algal production and trihalomethane formation potential: an experimental assessment and inter-river comparison. *Canadian Journal of Fisheries and Aquatic Sciences, 59*(9), 1482-1491.

Jiang, T., Skyllberg, U., Björn, E., Green, N. W., Tang, J., Wang, D., . . . Li, C. (2017). Characteristics of dissolved organic matter (DOM) and relationship with dissolved mercury in Xiaoqing River-Laizhou Bay estuary, Bohai Sea, China. *Environmental Pollution, 223*, 19-30.

Khamis, K., Bradley, C., Stevens, R., & Hannah, D. M. (2017). Continuous field estimation of dissolved organic carbon concentration and biochemical oxygen demand using dual ‐ wavelength fluorescence, turbidity and temperature. *Hydrological Processes, 31*(3), 540-555.

Korak, J. A., Wert, E. C., & Rosario-Ortiz, F. L. (2015). Evaluating fluorescence spectroscopy as a tool to characterize cyanobacteria intracellular organic matter upon simulated release and oxidation in natural water. *Water research, 68*, 432-443.

Kraus, T. E., Bergamaschi, B. A., Hernes, P. J., Doctor, D., Kendall, C., Downing, B. D., & Losee, R. F. (2011). How reservoirs alter drinking water quality: organic matter sources, sinks, and transformations. *Lake and Reservoir Management, 27*(3), 205-219.

Lambert, S., & Graham, N. (1995). Removal of non-specific dissolved organic matter from upland potable water supplies—II. Ozonation and adsorption. *Water Research, 29*(10), 2427-2433.

Lee, E.-J., Yoo, G.-Y., Jeong, Y., Kim, K.-U., Park, J.-H., & Oh, N.-H. (2015). Comparison of UV–VIS and FDOM sensors for in situ monitoring of stream DOC concentrations. *Biogeosciences, 12*(10), 3109-3118.

Leenheer, J. A., & Croué, J.-P. (2003). Peer reviewed: characterizing aquatic dissolved organic matter. In: ACS Publications.

Liungman, O., & Moreno-Arancibia, P. (2010). Developing a 3D coupled hydrodynamic and ecological model to be used in coastal management. In: Denmark: DHI.

Lu, J., Faggotter, S. J., Bunn, S. E., & Burford, M. A. (2017). Macrophyte beds in a subtropical reservoir shifted from a nutrient sink to a source after drying then rewetting. *Freshwater Biology, 62*(5), 854-867.

Mash, H., Westerhoff, P. K., Baker, L. A., Nieman, R. A., & Nguyen, M.-L. (2004). Dissolved organic matter in Arizona reservoirs: assessment of carbonaceous sources. *Organic Geochemistry, 35*(7), 831-843.

Mast, M. A., Murphy, S. F., Clow, D. W., Penn, C. A., & Sexstone, G. A. (2016). Water ‐ quality response to a high ‐ elevation wildfire in the Colorado Front Range. *Hydrological Processes, 30*(12), 1811-1823.

Mihalevich, B. A., Horsburgh, J. S., & Melcher, A. A. (2017). High-frequency measurements reveal spatial and temporal patterns of dissolved organic matter in an urban water conveyance. *Environmental Monitoring and Assessment, 189*(11), 593.

Moran, M. A., & Zepp, R. G. (1997). Role of photoreactions in the formation of biologically labile compounds from dissolved organic matter. *Limnology and oceanography, 42*(6), 1307-1316.

Mostofa, K. M. G. (2013). *Photobiogeochemistry of organic matter : principles and practices in water environments*. Heidelberg ; New York: Springer.

Pagano, T., Bida, M., & Kenny, J. E. (2014). Trends in levels of allochthonous dissolved organic carbon in natural water: A review of potential mechanisms under a changing climate. *Water*, *6*(10), 2862-2897.

Palmstrom, N. S., Carlson, R. E., & Cooke, G. D. (1988). Potential links between eutrophication and the formation of carcinogens in drinking water. *Lake and Reservoir Management*, *4*(2), 1-15.

Pellerin, B. A., Saraceno, J. F., Shanley, J. B., Sebestyen, S. D., Aiken, G. R., Wollheim, W. M., & Bergamaschi, B. A. (2012). Taking the pulse of snowmelt: in situ sensors reveal seasonal, event and diurnal patterns of nitrate and dissolved organic matter variability in an upland forest stream. *Biogeochemistry*, *108*(1-3), 183-198.

Ruhala, S. S., & Zarnetske, J. P. (2017). Using in-situ optical sensors to study dissolved organic carbon dynamics of streams and watersheds: A review. *Science of the Total Environment*, *575*, 713-723.

Saraceno, J. F., Pellerin, B. A., Downing, B. D., Boss, E., Bachand, P. A., & Bergamaschi, B. A. (2009). High‐frequency in situ optical measurements during a storm event: Assessing relationships between dissolved organic matter, sediment concentrations, and hydrologic processes. *Journal of Geophysical Research: Biogeosciences*, *114*(G4).

Saraceno, J. F., Shanley, J. B., Downing, B. D., & Pellerin, B. A. (2017). Clearing the waters: Evaluating the need for site‐specific field fluorescence corrections based on turbidity measurements. *Limnology and Oceanography: Methods*, *15*(4), 408-416.

Sato, T., Imazu, Y., Sakawa, T., Kazama, T., Wakabayashi, T., & Uhrenholdt, T. (2007). Modeling of integrated marine ecosystem including the generation-tracing type scallop growth model. *Ecological Modelling*, *208*(2), 263-285. doi:https://doi.org/10.1016/j.ecolmodel.2007.06.003

Stedmon, C. A., Thomas, D. N., Granskog, M., Kaartokallio, H., Papadimitriou, S., & Kuosa, H. (2007). Characteristics of dissolved organic matter in Baltic coastal sea ice: allochthonous or autochthonous origins? *Environmental Science & Technology*, *41*(21), 7273-7279.

Stutter, M., Dunn, S., & Lumsdon, D. (2012). Dissolved organic carbon dynamics in a UK podzolic moorland catchment: linking storm hydrochemistry, flow path analysis and sorption experiments. *Biogeosciences*, *9*(6), 2159-2175.

Tunaley, C., Tetzlaff, D., Lessels, J., & Soulsby, C. (2016). Linking high‐frequency DOC dynamics to the age of connected water sources. *Water Resources Research*, *52*(7), 5232-5247.

Tundisi, J. G., & Tundisi, T. M. (2012). *Limnology*: CRC Press.

Wang, X., Zhang, H., Bertone, E., Stewart, R. A., & O'Halloran, K. (2019). Analysis of the Mixing Processes in a Shallow Subtropical Reservoir and Their Effects on Dissolved Organic Matter. *Water*, *11*(4), 737. doi:https://doi.org/10.3390/w11040737

Wang, X., Zhang, H., Bertone, E., Stewart, R. A., & O'Halloran, K. (2020). Numerical Study of the Hydrodynamic and Sediment Transport Process in a Subtropical Water Reservoir: the Impacts of Storms and Winds. *Environmental Modeling & Assessment*. doi:10.1007/s10666-020-09719-5

Worrall, F., & Burt, T. (2010). Has the composition of fluvial DOC changed? Spatiotemporal patterns in the DOC‐color relationship. *Global biogeochemical cycles*, *24*(1).

Xylem. (2019). EXO User Manual. Advanced Water Quality Monitoring Platform.

Zepp, R., Erickson Iii, D., Paul, N., & Sulzberger, B. (2007). Interactive effects of solar UV radiation and climate change on biogeochemical cycling. *Photochemical & Photobiological Sciences*, *6*(3), 286-300.

Zhang, Y. L., Yin, Y., Liu, X. H., Shi, Z. Q., Feng, L. Q., Liu, M. L., . . . Qin, B. Q. (2012). Spatial‐seasonal dynamics of chromophoric dissolved organic matter in Lake Taihu, a large eutrophic, shallow lake in

China (vol 42, pg 510, 2011). *Organic Geochemistry*, *46*, 54-54. doi:10.1016/j.orggeochem.2012.02.002